

# Shape Matching and Object Recognition Using Shape Contexts

Serge Belongie, *Member, IEEE*, Jitendra Malik, *Member, IEEE*, and Jan Puzicha

**Abstract**—We present a novel approach to measuring similarity between shapes and exploit it for object recognition. In our framework, the measurement of similarity is preceded by 1) solving for correspondences between points on the two shapes, 2) using the correspondences to estimate an aligning transform. In order to solve the correspondence problem, we attach a descriptor, the *shape context*, to each point. The shape context at a reference point captures the distribution of the remaining points relative to it, thus offering a globally discriminative characterization. Corresponding points on two similar shapes will have similar shape contexts, enabling us to solve for correspondences as an optimal assignment problem. Given the point correspondences, we estimate the transformation that best aligns the two shapes; regularized thin-plate splines provide a flexible class of transformation maps for this purpose. The dissimilarity between the two shapes is computed as a sum of matching errors between corresponding points, together with a term measuring the magnitude of the aligning transform. We treat recognition in a nearest-neighbor classification framework as the problem of finding the stored prototype shape that is maximally similar to that in the image. Results are presented for silhouettes, trademarks, handwritten digits, and the COIL data set.

**Index Terms**—Shape, object recognition, digit recognition, correspondence problem, MPEG7, image registration, deformable templates.

## 1 INTRODUCTION

CONSIDER the two handwritten digits in Fig. 1. Regarded as vectors of pixel brightness values and compared using  $L_2$  norms, they are very different. However, regarded as *shapes* they appear rather similar to a human observer. Our objective in this paper is to operationalize this notion of shape similarity, with the ultimate goal of using it as a basis for category-level recognition. We approach this as a three-stage process:

1. solve the correspondence problem between the two shapes,
2. use the correspondences to estimate an aligning transform, and
3. compute the distance between the two shapes as a sum of matching errors between corresponding points, together with a term measuring the magnitude of the aligning transformation.

At the heart of our approach is a tradition of matching shapes by deformation that can be traced at least as far back as D'Arcy Thompson. In his classic work, *On Growth and Form* [55], Thompson observed that related but not identical shapes can often be deformed into alignment using simple

coordinate transformations, as illustrated in Fig. 2. In the computer vision literature, Fischler and Elschlager [15] operationalized such an idea by means of energy minimization in a mass-spring model. Grenander et al. [21] developed these ideas in a probabilistic setting. Yuille [61] developed another variant of the deformable template concept by means of fitting hand-crafted parametrized models, e.g., for eyes, in the image domain using gradient descent. Another well-known computational approach in this vein was developed by Lades et al. [31] using elastic graph matching.

Our primary contribution in this work is a robust and simple algorithm for finding correspondences between shapes. Shapes are represented by a set of points sampled from the shape contours (typically 100 or so pixel locations sampled from the output of an edge detector are used). There is nothing special about the points. They are *not* required to be landmarks or curvature extrema, etc.; as we use more samples, we obtain better approximations to the underlying shape. We introduce a shape descriptor, the *shape context*, to describe the coarse distribution of the rest of the shape with respect to a given point on the shape. Finding correspondences between two shapes is then equivalent to finding for each sample point on one shape the sample point on the other shape that has the most similar shape context. Maximizing similarities and enforcing uniqueness naturally leads to a setup as a bipartite graph matching (equivalently, optimal assignment) problem. As desired, we can incorporate other sources of matching information readily, e.g., similarity of local appearance at corresponding points.

Given the correspondences at sample points, we extend the correspondence to the complete shape by estimating an aligning transformation that maps one shape onto the other.

- S. Belongie is with the Department of Computer Science and Engineering, AP&M Building, Room 4832, University of California, San Diego, La Jolla, CA 92093-0114. E-mail: [sjb@cs.ucsd.edu](mailto:sjb@cs.ucsd.edu).
- J. Malik is with the Computer Science Division, University of California at Berkeley, 725 Soda Hall, Berkeley, CA 94720-1776. E-mail: [malik@cs.berkeley.edu](mailto:malik@cs.berkeley.edu).
- J. Puzicha is with RecomMind, Inc., 1001 Camelia St., Berkeley, CA 94710. E-mail: [jan@recommind.com](mailto:jan@recommind.com).

Manuscript received 09 Apr. 2001; revised 13 Aug. 2001; accepted 14 Aug. 2001.

Recommended for acceptance by J. Weng.

For information on obtaining reprints of this article, please send e-mail to: [tpami@computer.org](mailto:tpami@computer.org), and reference IEEECS Log Number 113957.



Fig. 1. Examples of two handwritten digits. In terms of pixel-to-pixel comparisons, these two images are quite different, but to the human observer, the shapes appear to be similar.

A classic illustration of this idea is provided in Fig. 2. The transformations can be picked from any of a number of families—we have used Euclidean, affine, and regularized thin plate splines in various applications. Aligning shapes enables us to define a simple, yet general, measure of shape similarity. The dissimilarity between the two shapes can now be computed as a sum of matching errors between corresponding points, together with a term measuring the magnitude of the aligning transform.

Given such a dissimilarity measure, we can use nearest-neighbor techniques for object recognition. Philosophically, nearest-neighbor techniques can be related to prototype-based recognition as developed by Rosch [47] and Rosch et al. [48]. They have the advantage that a vector space structure is not required—only a pairwise dissimilarity measure.

We demonstrate object recognition in a wide variety of settings. We deal with 2D objects, e.g., the MNIST data set of handwritten digits (Fig. 8), silhouettes (Figs. 11 and 13) and trademarks (Fig. 12), as well as 3D objects from the Columbia COIL data set, modeled using multiple views (Fig. 10). These are widely used benchmarks and our approach turns out to be the leading performer on all the problems for which there is comparative data.

We have also developed a technique for selecting the number of stored views for each object category based on its visual complexity. As an illustration, we show that for the 3D objects in the COIL-20 data set, one can obtain as low as 2.5 percent misclassification error using only an average of four views per object (see Figs. 9 and 10).

The structure of this paper is as follows: We discuss related work in Section 2. In Section 3, we describe our shape-matching method in detail. Our transformation model is presented in Section 4. We then discuss the problem of measuring shape similarity in Section 5 and demonstrate our proposed measure on a variety of

databases including handwritten digits and pictures of 3D objects in Section 6. We conclude in Section 7.

## 2 PRIOR WORK ON SHAPE MATCHING

Mathematicians typically define shape as an equivalence class under a group of transformations. This definition is incomplete in the context of visual analysis. This only tells us when two shapes are exactly the same. We need more than that for a theory of shape similarity or shape distance. The statistician's definition of shape, e.g., Bookstein [6] or Kendall [29], addresses the problem of shape distance, but assumes that correspondences are known. Other statistical approaches to shape comparison do not require correspondences—e.g., one could compare feature vectors containing descriptors such as area or moments—but such techniques often discard detailed shape information in the process. Shape similarity has also been studied in the psychology literature, an early example being Goldmeier [20].

An extensive survey of shape matching in computer vision can be found in [58], [22]. Broadly speaking, there are two approaches: 1) feature-based, which involve the use of spatial arrangements of extracted features such as edge elements or junctions, and 2) brightness-based, which make more direct use of pixel brightnesses.

### 2.1 Feature-Based Methods

A great deal of research on shape similarity has been done using the boundaries of *silhouette* images. Since silhouettes do not have holes or internal markings, the associated boundaries are conveniently represented by a single-closed curve which can be parametrized by arclength. Early work used Fourier descriptors, e.g., [62], [43]. Blum's medial axis transform has led to attempts to capture the part structure of the shape in the graph structure of the skeleton by Kimia, Zucker and collaborators, e.g., Sharvit et al. [53]. The 1D nature of silhouette curves leads naturally to dynamic programming approaches for matching, e.g., [17], which uses the edit distance between curves. This algorithm is fast and invariant to several kinds of transformation including some articulation and occlusion. A comprehensive comparison of different shape descriptors for comparing silhouettes was done as part of the MPEG-7 standard activity [33], with the leading approaches being those due to Latecki et al. [33] and Mokhtarian et al. [39].

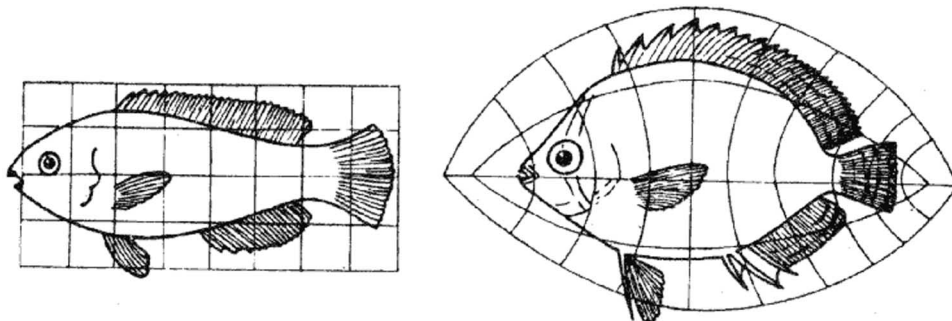


Fig. 2. Example of coordinate transformations relating two fish, from D'Arcy Thompson's *On Growth and Form* [55]. Thompson observed that similar biological forms could be related by means of simple mathematical transformations between *homologous* (i.e., corresponding) features. Examples of homologous features include center of eye, tip of dorsal fin, etc.

Silhouettes are fundamentally limited as shape descriptors for general objects; they ignore internal contours and are difficult to extract from real images. More promising are approaches that treat the shape as a set of points in the 2D image. Extracting these from an image is less of a problem—e.g., one can just use an edge detector. Huttenlocher et al. developed methods in this category based on the Hausdorff distance [23]; this can be extended to deal with partial matching and clutter. A drawback for our purposes is that the method does not return correspondences. Methods based on Distance Transforms, such as [16], are similar in spirit and behavior in practice.

The work of Sclaroff and Pentland [50] is representative of the eigenvector- or modal-matching based approaches; see also [52], [51], [57]. In this approach, sample points in the image are cast into a finite element spring-mass model and correspondences are found by comparing modes of vibration. Most closely related to our approach is the work of Gold et al. [19] and Chui and Rangarajan [9], which is discussed in Section 3.4.

There have been several approaches to shape recognition based on spatial configurations of a small number of keypoints or landmarks. In geometric hashing [32], these configurations are used to vote for a model without explicitly solving for correspondences. Amit et al. [1] train decision trees for recognition by learning discriminative spatial configurations of keypoints. Leung et al. [35], Schmid and Mohr [49], and Lowe [36] additionally use gray-level information at the keypoints to provide greater discriminative power. It should be noted that not all objects have distinguished key points (think of a circle for instance), and using key points alone sacrifices the shape information available in smooth portions of object contours.

## 2.2 Brightness-Based Methods

Brightness-based (or appearance-based) methods offer a complementary view to feature-based methods. Instead of focusing on the shape of the occluding contour or other extracted features, these approaches make direct use of the gray values within the visible portion of the object. One can use brightness information in one of two frameworks.

In the first category, we have the methods that explicitly find correspondences/alignment using grayscale values. Yuille [61] presents a very flexible approach in that invariance to certain kinds of transformations can be built into the measure of model similarity, but it suffers from the need for human-designed templates and the sensitivity to initialization when searching via gradient descent. Lades et al. [31] use elastic graph matching, an approach that involves both geometry and photometric features in the form of local descriptors based on Gaussian derivative jets. Vetter et al. [59] and Cootes et al. [10] compare brightness values but first attempt to warp the images onto one another using a dense correspondence field.

The second category includes those methods that build classifiers without explicitly finding correspondences. In such approaches, one relies on a learning algorithm having enough examples to acquire the appropriate invariances. In the area of face recognition, good results were obtained using principal components analysis (PCA) [54], [56] particularly

when used in a probabilistic framework [38]. Murase and Nayar applied these ideas to 3D object recognition [40]. Several authors have applied discriminative classification methods in the appearance-based shape matching framework. Some examples are the LeNet classifier [34], a convolutional neural network for handwritten digit recognition, and the Support Vector Machine (SVM)-based methods of [41] (for discriminating between templates of pedestrians based on 2D wavelet coefficients) and [11], [7] (for handwritten digit recognition). The MNIST database of handwritten digits is a particularly important data set as many different pattern recognition algorithms have been tested on it. We will show our results on MNIST in Section 6.1.

## 3 MATCHING WITH SHAPE CONTEXTS

In our approach, we treat an object as a (possibly infinite) point set and we assume that the shape of an object is essentially captured by a finite subset of its points. More practically, a shape is represented by a discrete set of points sampled from the internal or external contours on the object. These can be obtained as locations of edge pixels as found by an edge detector, giving us a set  $\mathcal{P} = \{p_1, \dots, p_n\}$ ,  $p_i \in \mathbb{R}^2$ , of  $n$  points. They need not, and typically will not, correspond to key-points such as maxima of curvature or inflection points. We prefer to sample the shape with roughly uniform spacing, though this is also not critical.<sup>1</sup> Figs. 3a and 3b show sample points for two shapes. Assuming contours are piecewise smooth, we can obtain as good an approximation to the underlying continuous shapes as desired by picking  $n$  to be sufficiently large.

### 3.1 Shape Context

For each point  $p_i$  on the first shape, we want to find the “best” matching point  $q_j$  on the second shape. This is a correspondence problem similar to that in stereopsis. Experience there suggests that matching is easier if one uses a rich local descriptor, e.g., a gray-scale window or a vector of filter outputs [27], instead of just the brightness at a single pixel or edge location. Rich descriptors reduce the ambiguity in matching.

As a key contribution, we propose a novel descriptor, the *shape context*, that could play such a role in shape matching. Consider the set of vectors originating from a point to all other sample points on a shape. These vectors express the configuration of the entire shape relative to the reference point. Obviously, this set of  $n - 1$  vectors is a rich description, since as  $n$  gets large, the representation of the shape becomes exact.

The full set of vectors as a shape descriptor is much too detailed since shapes and their sampled representation may vary from one instance to another in a category. We identify the *distribution* over relative positions as a more robust and compact, yet highly discriminative descriptor. For a point  $p_i$  on the shape, we compute a coarse histogram  $h_i$  of the relative coordinates of the remaining  $n - 1$  points,

$$h_i(k) = \#\{q \neq p_i : (q - p_i) \in \text{bin}(k)\}. \quad (1)$$

1. Sampling considerations are discussed in Appendix B.

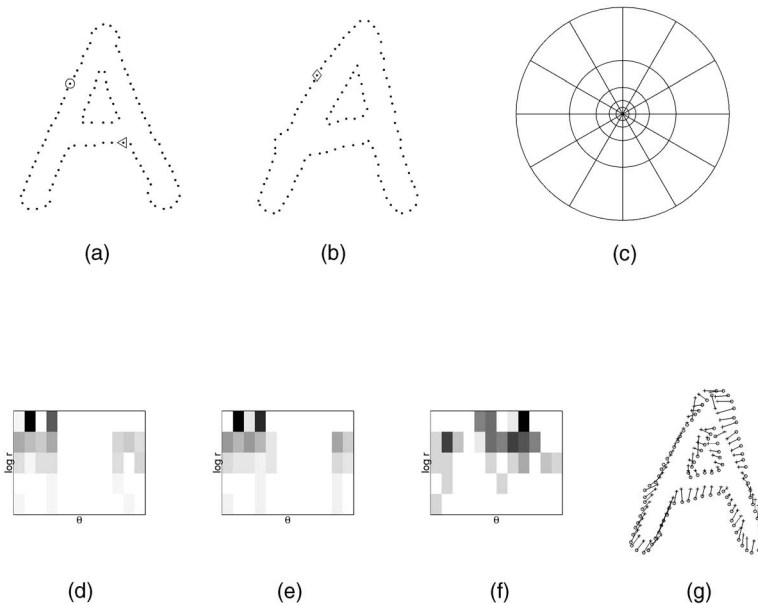


Fig. 3. Shape context computation and matching. (a) and (b) Sampled edge points of two shapes. (c) Diagram of log-polar histogram bins used in computing the shape contexts. We use five bins for  $\log r$  and 12 bins for  $\theta$ . (d), (e), and (f) Example shape contexts for reference samples marked by  $\circ$ ,  $\diamond$ ,  $\triangleleft$  in (a) and (b). Each shape context is a log-polar histogram of the coordinates of the rest of the point set measured using the reference point as the origin. (Dark=large value.) Note the visual similarity of the shape contexts for  $\circ$  and  $\diamond$ , which were computed for relatively similar points on the two shapes. By contrast, the shape context for  $\triangleleft$  is quite different. (g) Correspondences found using bipartite matching, with costs defined by the  $\chi^2$  distance between histograms.

This histogram is defined to be the *shape context* of  $p_i$ . We use bins that are uniform in log-polar<sup>2</sup> space, making the descriptor more sensitive to positions of nearby sample points than to those of points farther away. An example is shown in Fig. 3c.

Consider a point  $p_i$  on the first shape and a point  $q_j$  on the second shape. Let  $C_{ij} = C(p_i, q_j)$  denote the cost of matching these two points. As shape contexts are distributions represented as histograms, it is natural to use the  $\chi^2$  test statistic:

$$C_{ij} \equiv C(p_i, q_j) = \frac{1}{2} \sum_{k=1}^K \frac{[h_i(k) - h_j(k)]^2}{h_i(k) + h_j(k)},$$

where  $h_i(k)$  and  $h_j(k)$  denote the  $K$ -bin normalized histogram at  $p_i$  and  $q_j$ , respectively.<sup>3</sup>

The cost  $C_{ij}$  for matching points can include an additional term based on the local *appearance similarity* at points  $p_i$  and  $q_j$ . This is particularly useful when we are comparing shapes derived from gray-level images instead of line drawings. For example, one can add a cost based on normalized correlation scores between small gray-scale patches centered at  $p_i$  and  $q_j$ , distances between vectors of filter outputs at  $p_i$  and  $q_j$ , tangent orientation difference between  $p_i$  and  $q_j$ , and so on. The choice of this appearance similarity term is application dependent, and is driven by the necessary invariance and robustness requirements, e.g., varying lighting conditions make reliance on gray-scale brightness values risky.

2. This choice corresponds to a linearly increasing positional uncertainty with distance from  $p_i$ , a reasonable result if the transformation between the shapes around  $p_i$  can be locally approximated as affine.

3. Alternatives include Bickel's generalization of the Kolmogorov-Smirnov test for 2D distributions [4], which does not require binning.

### 3.2 Bipartite Graph Matching

Given the set of costs  $C_{ij}$  between all pairs of points  $p_i$  on the first shape and  $q_j$  on the second shape, we want to minimize the total cost of matching,

$$H(\pi) = \sum_i C(p_i, q_{\pi(i)}) \quad (2)$$

subject to the constraint that the matching be one-to-one, i.e.,  $\pi$  is a permutation. This is an instance of the square assignment (or weighted bipartite matching) problem, which can be solved in  $O(N^3)$  time using the Hungarian method [42]. In our experiments, we use the more efficient algorithm of [28]. The input to the assignment problem is a square cost matrix with entries  $C_{ij}$ . The result is a permutation  $\pi(i)$  such that (2) is minimized.

In order to have robust handling of outliers, one can add "dummy" nodes to each point set with a constant matching cost of  $\epsilon_d$ . In this case, a point will be matched to a "dummy" whenever there is no real match available at smaller cost than  $\epsilon_d$ . Thus,  $\epsilon_d$  can be regarded as a threshold parameter for outlier detection. Similarly, when the number of sample points on two shapes is not equal, the cost matrix can be made square by adding dummy nodes to the smaller point set.

### 3.3 Invariance and Robustness

A matching approach should be 1) invariant under scaling and translation, and 2) robust under small geometrical distortions, occlusion and presence of outliers. In certain applications, one may want complete invariance under rotation, or perhaps even the full group of affine transformations. We now evaluate shape context matching by these criteria.

Invariance to translation is intrinsic to the shape context definition since all measurements are taken with respect to points on the object. To achieve scale invariance we normalize all radial distances by the mean distance  $\alpha$  between the  $n^2$  point pairs in the shape.

Since shape contexts are extremely rich descriptors, they are inherently insensitive to small perturbations of parts of the shape. While we have no theoretical guarantees here, robustness to small nonlinear transformations, occlusions and presence of outliers is evaluated experimentally in Section 4.2.

In the shape context framework, we can provide for complete rotation invariance, if this is desirable for an application. Instead of using the absolute frame for computing the shape context at each point, one can use a relative frame, based on treating the tangent vector at each point as the positive  $x$ -axis. In this way, the reference frame turns with the tangent angle, and the result is a completely rotation invariant descriptor. In Appendix A, we demonstrate this experimentally. It should be emphasized though that, in many applications, complete invariance impedes recognition performance, e.g., when distinguishing 6 from 9 rotation invariance would be completely inappropriate. Another drawback is that many points will not have well-defined or reliable tangents. Moreover, many local appearance features lose their discriminative power if they are not measured in the same coordinate system.

Additional robustness to outliers can be obtained by excluding the estimated outliers from the shape context computation. More specifically, consider a set of points that have been labeled as outliers on a given iteration. We render these points “invisible” by not allowing them to contribute to any histogram. However, we still assign them shape contexts, taking into account only the surrounding inlier points, so that at a later iteration they have a chance of reemerging as an inlier.

### 3.4 Related Work

The most comprehensive body of work on shape correspondence in this general setting is the work of Gold et al. [19] and Chui and Rangarajan [9]. They developed an iterative optimization algorithm to determine point correspondences and underlying image transformations jointly, where typically some generic transformation class is assumed, e.g., affine or thin plate splines. The cost function that is being minimized is the sum of Euclidean distances between a point on the first shape and the *transformed* second shape. This sets up a chicken-and-egg problem: The distances make sense only when there is at least a rough alignment of shape. Joint estimation of correspondences and shape transformation leads to a difficult, highly non-convex optimization problem, which is solved using deterministic annealing [19]. The *shape context* is a very discriminative point descriptor, facilitating easy and robust correspondence recovery by incorporating global shape information into a local descriptor.

As far as we are aware, the shape context descriptor and its use for matching 2D shapes is novel. The most closely related idea in past work is that due to Johnson and Hebert [26] in their work on range images. They introduced a representation for matching dense clouds of oriented

3D points called the “spin image.” A spin image is a 2D histogram formed by spinning a plane around a normal vector on the surface of the object and counting the points that fall inside bins in the plane. As the size of this plane is relatively small, the resulting signature is not as informative as a shape context for purposes of recovering correspondences. This characteristic, however, might have the trade-off of additional robustness to occlusion. In another related work, Carlsson [8] has exploited the concept of *order structure* for characterizing local shape configurations. In this work, the relationships between points and tangent lines in a shape are used for recovering correspondences.

## 4 MODELING TRANSFORMATIONS

Given a finite set of correspondences between points on two shapes, one can proceed to estimate a plane transformation  $T: \mathbb{R}^2 \rightarrow \mathbb{R}^2$  that may be used to map arbitrary points from one shape to the other. This idea is illustrated by the warped gridlines in Fig. 2, wherein the specified correspondences consisted of a small number of landmark points such as the centers of the eyes, the tips of the dorsal fins, etc., and  $T$  extends the correspondences to arbitrary points.

We need to choose  $T$  from a suitable family of transformations. A standard choice is the affine model, i.e.,

$$T(x) = Ax + o \quad (3)$$

with some matrix  $A$  and a translational offset vector  $o$  parameterizing the set of all allowed transformations. Then, the least squares solution  $\hat{T} = (\hat{A}, \hat{o})$  is obtained by

$$\hat{o} = \frac{1}{n} \sum_{i=1}^n (p_i - q_{\pi(i)}), \quad (4)$$

$$\hat{A} = (Q^+ P)^t, \quad (5)$$

where  $P$  and  $Q$  contain the homogeneous coordinates of  $\mathcal{P}$  and  $\mathcal{Q}$ , respectively, i.e.,

$$P = \begin{pmatrix} 1 & p_{11} & p_{12} \\ \vdots & \vdots & \vdots \\ 1 & p_{n1} & p_{n2} \end{pmatrix}. \quad (6)$$

Here,  $Q^+$  denotes the pseudoinverse of  $Q$ .

In this work, we mostly use the thin plate spline (TPS) model [14], [37], which is commonly used for representing flexible coordinate transformations. Bookstein [6] found it to be highly effective for modeling changes in biological forms. Powell applied the TPS model to recover transformations between curves [44]. The thin plate spline is the 2D generalization of the cubic spline. In its regularized form, which is discussed below, the TPS model includes the affine model as a special case. We will now provide some background information on the TPS model.

We start with the 1D interpolation problem. Let  $v_i$  denote the target function values at corresponding locations  $p_i = (x_i, y_i)$  in the plane, with  $i = 1, 2, \dots, n$ . In particular, we will set  $v_i$  equal to  $x'_i$  and  $y'_i$  in turn to obtain one continuous transformation for each coordinate. We assume that the locations  $(x_i, y_i)$  are all different and are not collinear. The TPS interpolant  $f(x, y)$  minimizes the bending energy

$$I_f = \int \int_{\mathbb{R}^2} \left( \frac{\partial^2 f}{\partial x^2} \right)^2 + 2 \left( \frac{\partial^2 f}{\partial x \partial y} \right)^2 + \left( \frac{\partial^2 f}{\partial y^2} \right)^2 dx dy$$

and has the form:

$$f(x, y) = a_1 + a_x x + a_y y + \sum_{i=1}^n w_i U(\|(x_i, y_i) - (x, y)\|),$$

where the kernel function  $U(r)$  is defined by  $U(r) = r^2 \log r^2$  and  $U(0) = 0$  as usual. In order for  $f(x, y)$  to have square integrable second derivatives, we require that

$$\sum_{i=1}^n w_i = 0 \quad \text{and} \quad \sum_{i=1}^n w_i x_i = \sum_{i=1}^n w_i y_i = 0. \quad (7)$$

Together with the interpolation conditions,  $f(x_i, y_i) = v_i$ , this yields a linear system for the TPS coefficients:

$$\begin{pmatrix} K & P \\ P^T & 0 \end{pmatrix} \begin{pmatrix} w \\ a \end{pmatrix} = \begin{pmatrix} v \\ 0 \end{pmatrix} \quad (8)$$

where  $K_{ij} = U(\|(x_i, y_i) - (x_j, y_j)\|)$ , the  $i$ th row of  $P$  is  $(1, x_i, y_i)$ ,  $w$  and  $v$  are column vectors formed from  $w_i$  and  $v_i$ , respectively, and  $a$  is the column vector with elements  $a_1, a_x, a_y$ . We will denote the  $(n+3) \times (n+3)$  matrix of this system by  $L$ . As discussed, e.g., in [44],  $L$  is nonsingular and we can find the solution by inverting  $L$ . If we denote the upper left  $n \times n$  block of  $L^{-1}$  by  $A$ , then it can be shown that

$$I_f \propto v^T A v = w^T K w. \quad (9)$$

#### 4.1 Regularization and Scaling Behavior

When there is noise in the specified values  $v_i$ , one may wish to relax the exact interpolation requirement by means of regularization. This is accomplished by minimizing

$$H[f] = \sum_{i=1}^n (v_i - f(x_i, y_i))^2 + \lambda I_f. \quad (10)$$

The *regularization parameter*  $\lambda$ , a positive scalar, controls the amount of smoothing; the limiting case of  $\lambda = 0$  reduces to exact interpolation. As demonstrated in [60], [18], we can solve for the TPS coefficients in the regularized case by replacing the matrix  $K$  by  $K + \lambda I$ , where  $I$  is the  $n \times n$  identity matrix. It is interesting to note that the highly regularized TPS model degenerates to the least-squares affine model.

To address the dependence of  $\lambda$  on the data scale, suppose  $(x_i, y_i)$  and  $(x'_i, y'_i)$  are replaced by  $(\alpha x_i, \alpha y_i)$  and  $(\alpha x'_i, \alpha y'_i)$ , respectively, for some positive constant  $\alpha$ . Then, it can be shown that the parameters  $w, a, I_f$  of the optimal thin plate spline are unaffected if  $\lambda$  is replaced by  $\alpha^2 \lambda$ . This simple scaling behavior suggests a normalized definition of the regularization parameter. Let  $\alpha$  again represent the scale of the point set as estimated by the mean edge length between two points in the set. Then, we can define  $\lambda$  in terms of  $\alpha$  and  $\lambda_o$ , a scale-independent regularization parameter, via the simple relation  $\lambda = \alpha^2 \lambda_o$ .

We use two separate TPS functions to model a coordinate transformation,

$$T(x, y) = (f_x(x, y), f_y(x, y)) \quad (11)$$

which yields a displacement field that maps any position in the first image to its interpolated location in the second image.

In many cases, the initial estimate of the correspondences contains some errors which could degrade the quality of the transformation estimate. The steps of recovering correspondences and estimating transformations can be iterated to overcome this problem. We usually use a fixed number of iterations, typically three in large-scale experiments, but more refined schemes are possible. However, experimental experiences show that the algorithmic performance is independent of the details. An example of the iterative algorithm is illustrated in Fig. 4.

#### 4.2 Empirical Robustness Evaluation

In order to study the robustness of our proposed method, we performed the synthetic point set matching experiments described in [9]. The experiments are broken into three parts designed to measure robustness to deformation, noise, and outliers. (The latter tests each include a “moderate” amount of deformation.) In each test, we subjected the model point set to one of the above distortions to create a “target” point set; see Fig. 5. We then ran our algorithm to find the best warping between the model and the target. Finally, the performance is quantified by computing the average distance between the coordinates of the warped model and those of the target. The results are shown in Fig. 6. In the most challenging part of the test—the outlier experiment—our approach shows robustness even up to a level of 100 percent outlier-to-data ratio.

In practice, we will need robustness to occlusion and segmentation errors which can be explored only in the context of a complete recognition system, though these experiments provide at least some guidelines.

#### 4.3 Computational Demands

In our implementation on a regular Pentium III /500 MHz workstation, a single comparison including computation of shape context for 100 sample points, set-up of the full matching matrix, bipartite graph matching, computation of the TPS coefficients, and image warping for three cycles takes roughly 200ms. The runtime is dominated by the number of sample points for each shape, with most components of the algorithm exhibiting between quadratic and cubic scaling behavior. Using a sparse representation throughout, once the shapes are roughly aligned, the complexity could be made close to linear.

### 5 OBJECT RECOGNITION AND PROTOTYPE SELECTION

Given a measure of dissimilarity between shapes, which we will make precise shortly, we can proceed to apply it to the task of object recognition. Our approach falls into the category of prototype-based recognition. In this framework, pioneered by Rosch et al. [48], categories are represented by ideal

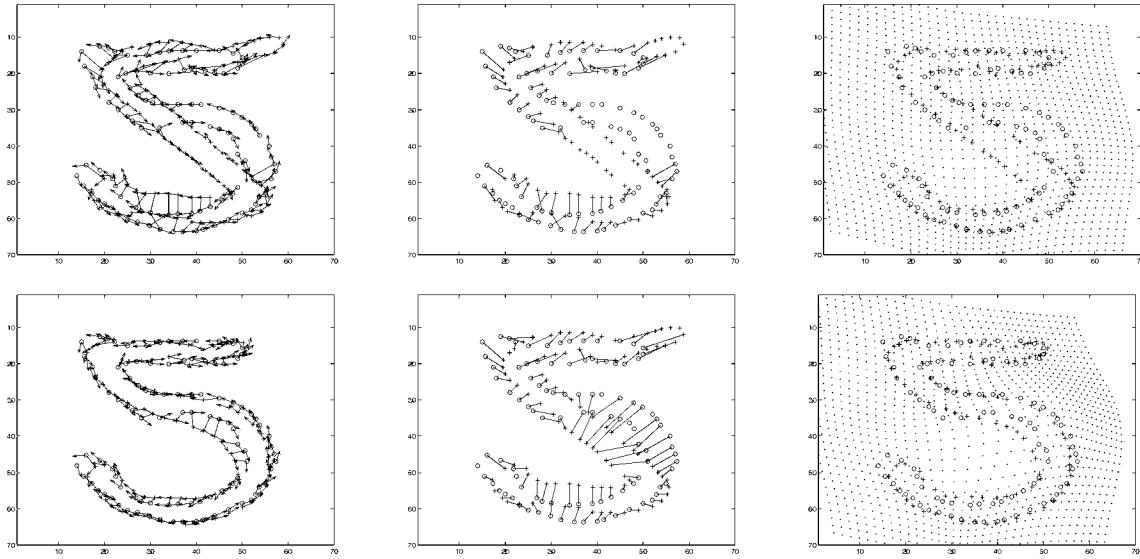


Fig. 4. Illustration of the matching process applied to the example of Fig. 1. Top row: 1st iteration. Bottom row: 5th iteration. Left column: estimated correspondences shown relative to the transformed model, with tangent vectors shown. Middle column: estimated correspondences shown relative to the untransformed model. Right column: result of transforming the model based on the current correspondences; this is the input to the next iteration. The grid points illustrate the interpolated transformation over  $\mathbb{R}^2$ . Here, we have used a regularized TPS model with  $\lambda_0 = 1$ .

examples rather than a set of formal logical rules. As an example, a sparrow is a likely prototype for the category of birds; a less likely choice might be an penguin. The idea of prototypes allows for soft category membership, meaning that as one moves farther away from the ideal example in some suitably defined similarity space, one's association with that prototype falls off. When one is sufficiently far away from that prototype, the distance becomes meaningless, but by then one is most likely near a different prototype. As an example, one can talk about good or so-so examples of the color red, but when the color becomes sufficiently different, the level of dissimilarity saturates at some maximum level rather than continuing on indefinitely.

Prototype-based recognition translates readily into the computational framework of nearest-neighbor methods using multiple stored views. Nearest-neighbor classifiers have the property [46] that as the number of examples  $n$  in the training set goes to infinity, the 1-NN error converges to a value  $\leq 2E^*$ , where  $E^*$  is the Bayes Risk (for  $K$ -NN,  $K \rightarrow$

$\infty$  and  $K/n \rightarrow 0$ , the error  $\rightarrow E^*$ ). This is interesting because it shows that the humble nearest-neighbor classifier is asymptotically optimal, a property not possessed by several considerably more complicated techniques. Of course, what matters in practice is the performance for small  $n$ , and this gives us a way to compare different similarity/distance measures.

### 5.1 Shape Distance

In this section, we make precise our definition of shape distance and apply it to several practical problems. We used a regularized TPS transformation model and three iterations of shape context matching and TPS reestimation. After matching, we estimated shape distances as the weighted sum of three terms: shape context distance, image appearance distance, and bending energy.

We measure shape context distance between shapes  $\mathcal{P}$  and  $\mathcal{Q}$  as the symmetric sum of shape context matching costs over best matching points, i.e.,

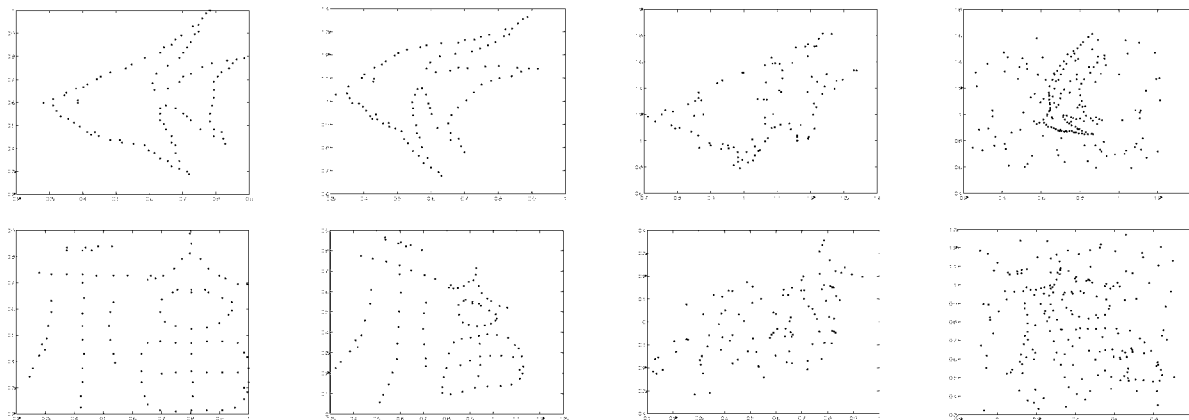


Fig. 5. Testing data for empirical robustness evaluation, following Chui and Rangarajan [9]. The model pointsets are shown in the first column. Columns 2-4 show examples of target point sets for the deformation, noise, and outlier tests, respectively.

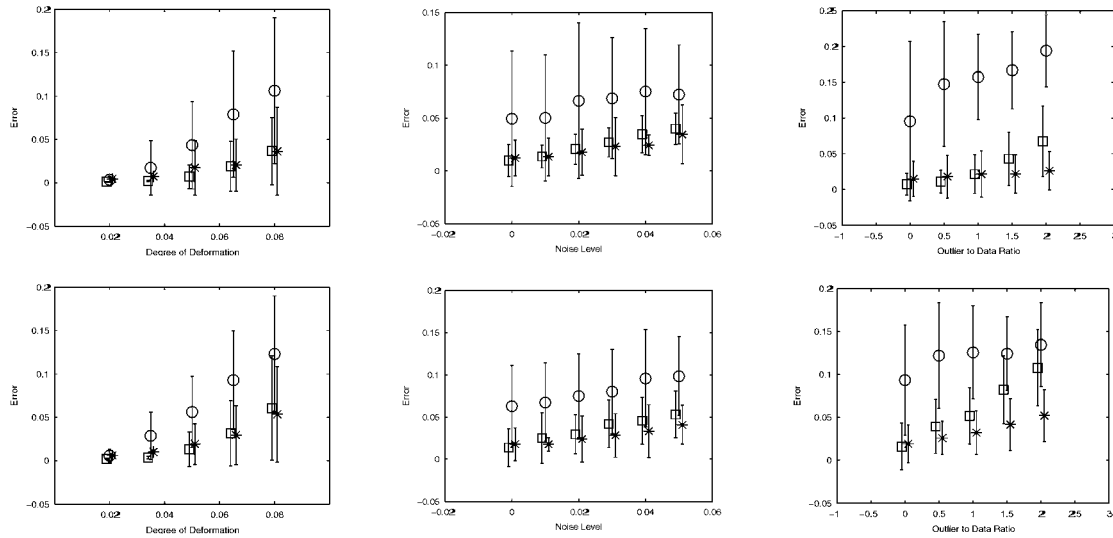


Fig. 6. Comparison of our results ( $\square$ ) to Chui and Rangarajan (\*) and iterated closest point ( $\circ$ ) for the fish and Chinese character, respectively. The error bars indicate the standard deviation of the error over 100 random trials. Here, we have used 5 iterations with  $\lambda_o = 1.0$ . In the deformation and noise tests no dummy nodes were added. In the outlier test, dummy nodes were added to the model point set such that the total number of nodes was equal to that of the target. In this case, the value of  $\epsilon_d$  does not affect the solution.

$$\mathcal{D}_{sc}(\mathcal{P}, \mathcal{Q}) = \frac{1}{n} \sum_{p \in \mathcal{P}} \arg \min_{q \in \mathcal{Q}} C(p, T(q)) + \frac{1}{m} \sum_{q \in \mathcal{Q}} \arg \min_{p \in \mathcal{P}} C(p, T(q)), \quad (12)$$

where  $T(\cdot)$  denotes the estimated TPS shape transformation.

In many applications there is additional appearance information available that is not captured by our notion of shape, e.g., the texture and color information in the grayscale image patches surrounding corresponding points. The reliability of appearance information often suffers substantially from geometric image distortions. However, after establishing image correspondences and recovery of underlying 2D image transformation the distorted image can be warped back into a normal form, thus correcting for distortions of the image appearance.

We used a term  $\mathcal{D}_{ac}(\mathcal{P}, \mathcal{Q})$  for appearance cost, defined as the sum of squared brightness differences in Gaussian windows around corresponding image points,

$$\mathcal{D}_{ac}(\mathcal{P}, \mathcal{Q}) = \frac{1}{n} \sum_{i=1}^n \sum_{\Delta \in \mathbb{Z}^2} G(\Delta) [I_{\mathcal{P}}(p_i + \Delta) - I_{\mathcal{Q}}(T(q_{\pi(i)}) + \Delta)]^2, \quad (13)$$

where  $I_{\mathcal{P}}$  and  $I_{\mathcal{Q}}$  are the gray-level images corresponding to  $\mathcal{P}$  and  $\mathcal{Q}$ , respectively.  $\Delta$  denotes some differential vector offset and  $G$  is a windowing function typically chosen to be a Gaussian, thus putting emphasis to pixels nearby. We thus sum over squared differences in windows around corresponding points, scoring the weighted gray-level similarity.

This score is computed *after* the thin plate spline transformation  $T$  has been applied to best warp the images into alignment.

The third term  $\mathcal{D}_{be}(\mathcal{P}, \mathcal{Q})$  corresponds to the “amount” of transformation necessary to align the shapes. In the TPS case the bending energy (9) is a natural measure (see [5]).

## 5.2 Choosing Prototypes

In a prototype-based approach, the key question is: what examples shall we store? Different categories need different numbers of views. For example, certain handwritten digits have more variability than others, e.g., one typically sees more variations in fours than in zeros. In the category of 3D objects, a sphere needs only one view, for example, while a telephone needs several views to capture the variety of visual appearance. This idea is related to the “aspect” concept as discussed in [30]. We will now discuss how we approach the problem of prototype selection.

In the nearest-neighbor classifier literature, the problem of selecting exemplars is called *editing*. Extensive reviews of nearest-neighbor editing methods can be found in Ripley [46] and Dasarthy [12]. We have developed a novel editing algorithm based on shape distance and  $K$ -medoids clustering.  $K$ -medoids can be seen as a variant of  $K$ -means that restricts prototype positions to data points. First a matrix of pairwise similarities between all possible prototypes is computed. For a given number of  $K$  prototypes the  $K$ -medoids algorithm then iterates two steps: 1) For a given assignment of points to (abstract) clusters a new prototype is selected for that cluster by minimizing the average distance of the prototype to all elements in the cluster, and 2) given the set of prototypes, points are then reassigned to clusters according to the nearest prototype. More formally, denote by  $c(\mathcal{P})$  the (abstract) cluster of shape  $\mathcal{P}$ , e.g., represented by some number  $\{1, \dots, k\}$  and denote by  $p(c)$  the associated prototype. Thus, we have a class map

$$c: \mathcal{S}_1 \subset \mathcal{S} \longrightarrow \{1, \dots, k\} \quad (14)$$

and a prototype map

$$p: \{1, \dots, k\} \longrightarrow \mathcal{S}_2 \subset \mathcal{S}. \quad (15)$$

Here,  $\mathcal{S}_1$  and  $\mathcal{S}_2$  are some subsets of the set of all potential shapes  $\mathcal{S}$ . Often,  $\mathcal{S} = \mathcal{S}_1 = \mathcal{S}_2$ .  $K$ -medoids proceeds by iterating two steps:



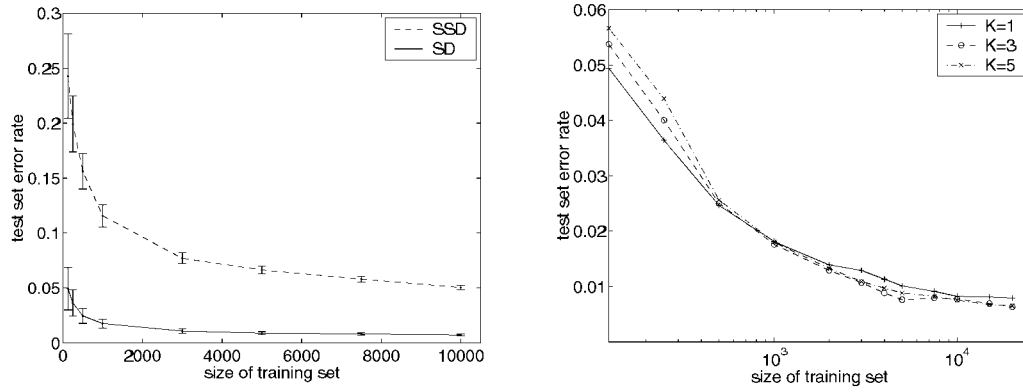


Fig. 7. Handwritten digit recognition on the MNIST data set. Left: Test set errors of a 1-NN classifier using SSD and Shape Distance (SD) measures. Right: Detail of performance curve for Shape Distance, including results with training set sizes of 15,000 and 20,000. Results are shown on a semilog-x scale for  $K = 1, 3, 5$  nearest-neighbors.

1. group  $S_1$  into classes given the class prototypes  $p(c)$ , and
2. identify a representative prototype for each class given the elements in the cluster.

Basically, item 1 is solved by assigning each shape  $P \in S_1$  to the nearest prototype, thus

$$c(P) = \arg \min_k \mathcal{D}(P, p(k)). \quad (16)$$

For given classes, in item 2 new prototypes are selected based on minimal mean dissimilarity, i.e.,

$$p(k) = \arg \min_{p \in S_2} \sum_{P: c(P)=k} \mathcal{D}(P, p). \quad (17)$$

Since both steps minimize the same cost function

$$H(c, p) = \sum_{P \in S_1} \mathcal{D}(P, p(c(P))), \quad (18)$$

the algorithm necessarily converges to a (local) minimum.

As with most clustering methods, with  $k$ -medoids one must have a strategy for choosing  $k$ . We select the number of prototypes using a greedy splitting strategy starting with one prototype per category. We choose the cluster to split based on the associated overall misclassification error. This continues until the overall misclassification error has dropped below a criterion level. Thus, the prototypes are automatically allocated to the different object classes, thus optimally using available resources. The application of this procedure to a set of views of 3D objects is explored in Section 6.2 and illustrated in Fig. 10.

## 6 CASE STUDIES

### 6.1 Digit Recognition

Here, we present results on the MNIST data set of handwritten digits, which consists of 60,000 training and 10,000 test digits [34]. In the experiments, we used 100 points sampled from the Canny edges to represent each digit. When computing the  $C_{ij}^{\tan}$ 's for the bipartite matching, we included a term representing the dissimilarity of local tangent angles. Specifically, we defined the matching cost as  $C_{ij} = (1 - \beta)C_{ij}^{sc} + \beta C_{ij}^{\tan}$ , where  $C_{ij}^{sc}$  is the shape context cost,

$C_{ij}^{\tan} = 0.5(1 - \cos(\theta_i - \theta_j))$  measures tangent angle dissimilarity, and  $\beta = 0.1$ . For recognition, we used a  $K$ -NN classifier with a distance function

$$\mathcal{D} = 1.6\mathcal{D}_{ac} + \mathcal{D}_{sc} + 0.3\mathcal{D}_{be}. \quad (19)$$

The weights in (19) have been optimized by a leave-one-out procedure on a  $3,000 \times 3,000$  subset of the training data.

On the MNIST data set nearly 30 algorithms have been compared (<http://www.research.att.com/~yann/exdb/mnist/index.html>). The lowest test set error rate published at this time is 0.7 percent for a boosted LeNet-4 with a training set of size  $60,000 \times 10$  synthetic distortions per training digit. Our error rate using 20,000 training examples and 3-NN is 0.63 percent. The 63 errors are shown in Fig. 8.<sup>4</sup>

As mentioned earlier, what matters in practical applications of nearest-neighbor methods is the performance for small  $n$ , and this gives us a way to compare different similarity/distance measures. In Fig. 7 (left), our shape distance is compared to SSD (sum of squared differences between pixel brightness values). In Fig. 7 (right), we compare the classification rates for different  $K$ .

### 6.2 3D Object Recognition

Our next experiment involves the 20 common household objects from the COIL-20 database [40]. Each object was placed on a turntable and photographed every  $5^\circ$  for a total of 72 views per object. We prepared our training sets by selecting a number of equally spaced views for each object and using the remaining views for testing. The matching algorithm is exactly the same as for digits. Recall, that the Canny edge detector responds both to external and internal contours, so the 100 sample points are not restricted to the external boundary of the silhouette.

Fig. 9 shows the performance using 1-NN with the distance function  $D$  as given in (19) compared to a

<sup>4</sup> DeCoste and Schölkopf [13] report an error rate of 0.56 percent on the same database using Virtual Support Vectors (VSV) with the full training set of 60,000. VSVs are found as follows: 1) obtain SVs from the original training set using a standard SVM, 2) subject the SVs to a set of desired transformations (e.g., translation), 3) train another SVM on the generated examples.

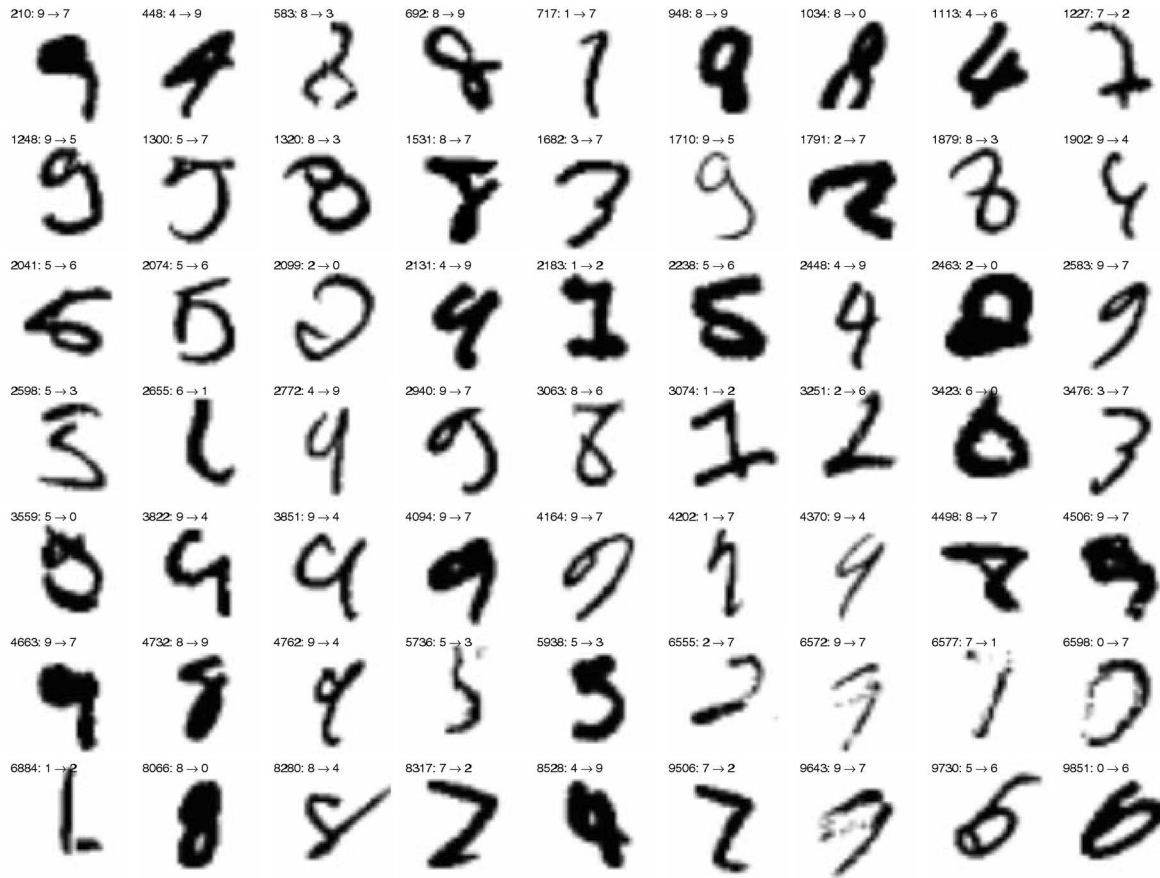


Fig. 8. All of the misclassified MNIST test digits using our method (63 out of 10,000). The text above each digit indicates the example number followed by the true label and the assigned label.

straightforward sum of squared differences (SSD). SSD performs very well on this easy database due to the lack of variation in lighting [24] (PCA just makes it faster).

The prototype selection algorithm is illustrated in Fig. 10. As seen, views are allocated mainly for more complex categories with high within class variability. The curve marked SC-proto in Fig. 9 shows the improved classification performance using this prototype selection strategy instead of equally-spaced views. Note that we obtain a 2.4 percent

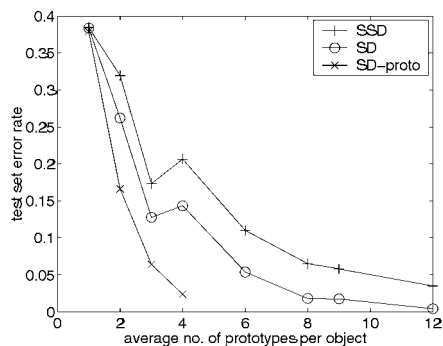


Fig. 9. 3D object recognition using the COIL-20 data set. Comparison of test set error for SSD, Shape Distance (SD), and Shape Distance with  $k$ -medoids prototypes (SD-proto) versus number of prototype views. For SSD and SD, we varied the number of prototypes uniformly for all objects. For SD-proto, the number of prototypes per object depended on the within-object variation as well as the between-object similarity.

error rate with an average of only four two-dimensional views for each three-dimensional object, thanks to the flexibility provided by the matching algorithm.

### 6.3 MPEG-7 Shape Silhouette Database

Our next experiment involves the MPEG-7 shape silhouette database, specifically Core Experiment CE-Shape-1 part B, which measures performance of similarity-based retrieval [25]. The database consists of 1,400 images: 70 shape categories, 20 images per category. The performance is measured using the so-called “bullseye test,” in which each



Fig. 10. Prototype views selected for two different 3D objects from the COIL data set using the algorithm described in Section 5.2. With this approach, views are allocated adaptively depending on the visual complexity of an object with respect to viewing angle.

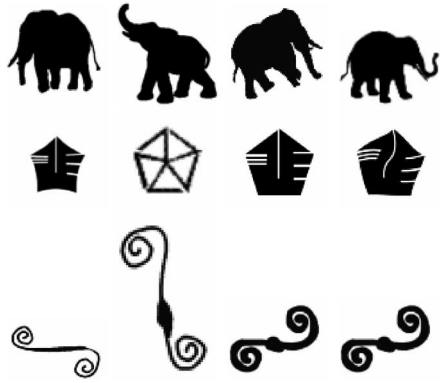


Fig. 11. Examples of shapes in the MPEG7 database for three different categories.

image is used as a query and one counts the number of correct images in the top 40 matches.

As this experiment involves intricate shapes we increased the number of samples from 100 to 300. In some categories, the shapes appear rotated and flipped, which we address using a modified distance function. The distance  $\text{dist}(R, Q)$  between a reference shape  $R$  and a query shape  $Q$  is defined as

$$\text{dist}(Q, R) = \min\{\text{dist}(Q, R^a), \text{dist}(Q, R^b), \text{dist}(Q, R^c)\},$$

where  $R^a$ ,  $R^b$ , and  $R^c$  denote three versions of  $R$ : unchanged, vertically flipped, and horizontally flipped.

With these changes in place but otherwise using the same approach as in the MNIST digit experiments, we obtain a retrieval rate of 76.51 percent. Currently the best published performance is achieved by Latecki et al. [33], with a retrieval rate of 76.45 percent, followed by Mokhtarian et al. at 75.44 percent.

#### 6.4 Trademark Retrieval

Trademarks are visually often best described by their shape information, and, in many cases, shape provides the only source of information. The automatic identification of trademark infringement has interesting industrial applications, since with the current state of the art trademarks are broadly categorized according to the Vienna code, and then manually classified according to their perceptual similarity. Even though shape context matching does not provide a full solution to the trademark similarity problem (other potential cues are text and texture), it still serves well to illustrate the capability of our approach to capture the essence of shape similarity. In Fig. 12, we depict retrieval results for a database of 300 trademarks. In this experiment, we relied on an affine transformation model as given by (3), and as in the previous case, we used 300 sample points.

We experimented with eight different query trademarks for each of which the database contained at least one potential infringement. We depict the top four hits as well as their similarity score. It is clearly seen that the potential infringements are easily detected and appear as most similar in the top ranks despite substantial variation of the actual shapes. It has been manually verified that no visually similar trademark has been missed by the algorithm.

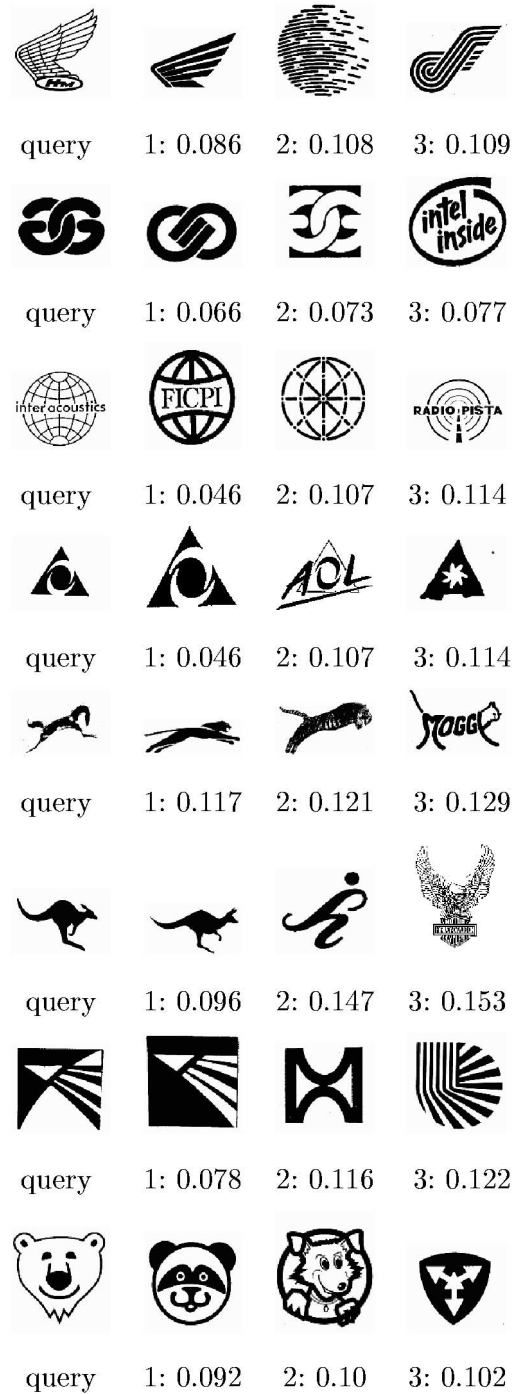


Fig. 12. Trademark retrieval results based on a database of 300 different real-world trademarks. We used an affine transformation model and a weighted combination of shape context similarity  $D_{sc}$  and the sum over local tangent orientation differences.

#### 7 CONCLUSION

We have presented a new approach to shape matching. A key characteristic of our approach is the estimation of shape similarity and correspondences based on a novel descriptor, the shape context. Our approach is simple and easy to apply, yet provides a rich descriptor for point sets that greatly improves point set registration, shape matching and shape recognition. In our experiments, we have demonstrated

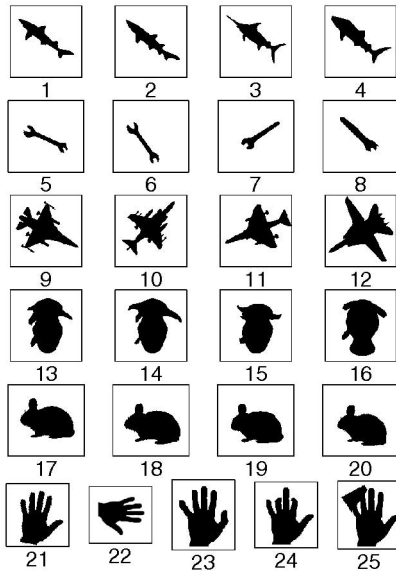


Fig. 13. Kimia data set: each row shows instances of a different object category. Performance is measured by the number of closest matches with the correct category label. Note that several of the categories require rotation invariant matching for effective recognition. All of the 1st ranked closest matches were correct using our method. Of the 2nd ranked matches, one error occurred in 1 versus 8. In the 3rd ranked matches, confusions arose from 2 versus 8, 8 versus 1, and 15 versus 17.

invariance to several common image transformations, including significant 3D rotations of real-world objects.

## APPENDIX A

### COMPLETE ROTATION INVARIANT RECOGNITION

In this appendix, we demonstrate the use of the relative frame in our approach as a means of obtaining complete rotation invariance. To demonstrate this idea, we have used the database provided by Sharvit et al. [53] shown in Fig. 13. In this experiment, we used  $n = 100$  sample points and, as mentioned above, we used the relative frame (Section 3.3) when computing the shape contexts. We used five bins for  $\log(r)$  over the range  $0.125\alpha$  to  $2\alpha$  and 12 equally spaced radial bins in these and all other experiments in this paper. No transformation model at all was used. As a similarity score, we used the matching cost function  $\sum_i C_{i,\pi(i)}$  after one iteration with no transformation step. Thus, this experiment is specifically designed solely to evaluate the power of the shape descriptor in the face of rotation.

In [53] and [17], the authors summarize their results on this data set by stating the number of 1st, 2nd, and 3rd nearest-neighbors that fall into the correct category. Our results are 25/25, 24/25, 22/25. In [53] and [17], the results quoted are 23/25, 21/25, 20/25 and 25/25, 21/25, 19/25, respectively.

## APPENDIX B

### SAMPLING CONSIDERATIONS

In our approach, a shape is represented by a set of sample points drawn from the internal and external contours of an object. Operationally, one runs an edge detector on the

gray-scale image and selects a subset of the edge pixels found. The selection could be uniformly at random, but we have found it to be advantageous to ensure that the sample points have a certain minimum distance between them as this makes sure that the sampling along the contours is somewhat uniform. (This corresponds to sampling from a point process which is a hard-core model [45].)

Since the sample points are drawn randomly and independently from the two shapes, there is inevitably jitter noise in the output of the matching algorithm which finds correspondences between these two sets of sample points. However, when the transformation between the shapes is estimated as a regularized thin plate spline, the effect of this jitter is smoothed away.

## ACKNOWLEDGMENTS

This research is supported by the Army Research Office (ARO) DAAH04-96-1-0341, the Digital Library Grant IRI-9411334, a US National Science Foundation Graduate Fellowship for S. Belongie, and the German Research Foundation by DFG grant PU-165/1. Parts of this work have appeared in [3], [2]. The authors wish to thank H. Chui and A. Rangarajan for providing the synthetic testing data used in Section 4.2. We would also like to thank them and various members of the Berkeley computer vision group, particularly A. Berg, A. Efros, D. Forsyth, T. Leung, J. Shi, and Y. Weiss, for useful discussions. This work was carried out while the authors were with the Department of Electrical Engineering and Computer Science Division, University of California at Berkeley.

## REFERENCES

- [1] Y. Amit, D. Geman, and K. Wilder, "Joint Induction of Shape Features and Tree Classifiers," *IEEE Trans. Pattern Analysis and Machine Intelligence*, vol. 19, no. 11, pp. 1300-1305, Nov. 1997.
- [2] S. Belongie, J. Malik, and J. Puzicha, "Matching Shapes," *Proc. Eighth Int'l. Conf. Computer Vision*, pp. 454-461, July 2001.
- [3] S. Belongie, J. Malik, and J. Puzicha, "Shape Context: A New Descriptor for Shape Matching and Object Recognition," *Advances in Neural Information Processing Systems 13: Proc. 2000 Conf.*, T.K. Leen, T.G. Dietterich, and V. Tresp, eds., pp. 831-837, 2001.
- [4] P.J. Bickel, "A Distribution Free Version of the Smirnov Two-Sample Test in the Multivariate Case," *Annals of Math. Statistics*, vol. 40, pp. 1-23, 1969.
- [5] F.L. Bookstein, "Principal Warps: Thin-Plate Splines and Decomposition of Deformations," *IEEE Trans. Pattern Analysis and Machine Intelligence*, vol. 11, no. 6, pp. 567-585, June 1989.
- [6] F.L. Bookstein, *Morphometric Tools for Landmark Data: Geometry and Biology*. Cambridge Univ. Press, 1991.
- [7] C. Burges and B. Schölkopf, "Improving the Accuracy and Speed of Support Vector Machines," *Advances in Neural Information Processing Systems 9: Proc. 1996 Conf.*, D.S. Touretzky, M.C. Mozer, and M. E. Hasselmo, eds., pp. 375-381, 1997.
- [8] S. Carlsson, "Order Structure, Correspondence and Shape Based Categories," *Int'l Workshop Shape, Contour and Grouping*, May 1999.
- [9] H. Chui and A. Rangarajan, "A New Algorithm for Non-Rigid Point Matching," *Proc. IEEE Conf. Computer Vision and Pattern Recognition*, pp. 44-51, June 2000.
- [10] T. Coates, D. Cooper, C. Taylor, and J. Graham, "Active Shape Models—Their Training and Application," *Computer Vision and Image Understanding (CVIU)*, vol. 61, no. 1, pp. 38-59, Jan. 1995.
- [11] C. Cortes and V. Vapnik, "Support Vector Networks," *Machine Learning*, vol. 20, pp. 273-297, 1995.
- [12] *Nearest Neighbor (NN) Norms: (NN) Pattern Classification Techniques*. B.V. Dasarthy, ed., IEEE Computer Soc., 1991.

- [13] D. DeCoste and B. Schölkopf, "Training Invariant Support Vector Machines," *Machine Learning*, to appear in 2002.
- [14] J. Duchon, "Splines Minimizing Rotation-Invariant Semi-Norms in Sobolev Spaces," *Constructive Theory of Functions of Several Variables*, W. Schempp and K. Zeller, eds., pp. 85-100, Berlin: Springer-Verlag, 1977.
- [15] M. Fischler and R. Elschlager, "The Representation and Matching of Pictorial Structures," *IEEE Trans. Computers*, vol. 22, no. 1, pp. 67-92, 1973.
- [16] D. Gavrila and V. Philomin, "Real-Time Object Detection for Smart Vehicles," *Proc. Seventh Int'l. Conf. Computer Vision*, pp. 87-93, 1999.
- [17] Y. Gdalyahu and D. Weinshall, "Flexible Syntactic Matching of Curves and its Application to Automatic Hierarchical Classification of Silhouettes," *IEEE Trans. Pattern Analysis and Machine Intelligence*, vol. 21, no. 12, pp. 1312-1328, Dec. 1999.
- [18] F. Girosi, M. Jones, and T. Poggio, "Regularization Theory and Neural Networks Architectures," *Neural Computation*, vol. 7, no. 2, pp. 219-269, 1995.
- [19] S. Gold, A. Rangarajan, C.-P. Lu, S. Pappu, and E. Mjolsness, "New Algorithms for 2D and 3D Point Matching: Pose Estimation and Correspondence," *Pattern Recognition*, vol. 31, no. 8, 1998.
- [20] E. Goldmeier, "Similarity in Visually Perceived Forms," *Psychological Issues*, vol. 8, no. 1, pp. 1-135, 1936/1972.
- [21] U. Grenander, Y. Chow, and D. Keenan, *HANDS: A Pattern Theoretic Study Of Biological Shapes*. Springer, 1991.
- [22] M. Hagedoorn, "Pattern Matching Using Similarity Measures," PhD thesis, Universiteit Utrecht, 2000.
- [23] D. Huttenlocher, G. Klanderman, and W. Rucklidge, "Comparing Images Using the Hausdorff Distance," *IEEE Trans. Pattern Analysis and Machine Intelligence*, vol. 15, no. 9, pp. 850-863, Sept. 1993.
- [24] D. Huttenlocher, R. Lilien, and C. Olson, "View-Based Recognition Using an Eigenspace Approximation to the Hausdorff Measure," *IEEE Trans. Pattern Analysis and Machine Intelligence*, vol. 21, no. 9, pp. 951-955, Sept. 1999.
- [25] S. Jeannin and M. Bober, "Description of Core Experiments for MPEG-7 Motion/Shape," Technical Report ISO/IEC JTC 1/SC 29/WG 11 MPEG99/N2690, MPEG-7, Seoul, Mar. 1999.
- [26] A.E. Johnson and M. Hebert, "Recognizing Objects by Matching Oriented Points," *Proc. IEEE Conf. Computer Vision and Pattern Recognition*, pp. 684-689, 1997.
- [27] D. Jones and J. Malik, "Computational Framework to Determining Stereo Correspondence from a Set of Linear Spatial Filters," *Image and Vision Computing*, vol. 10, no. 10, pp. 699-708, Dec. 1992.
- [28] R. Jonker and A. Volgenant, "A Shortest Augmenting Path Algorithm for Dense and Sparse Linear Assignment Problems," *Computing*, vol. 38, pp. 325-340, 1987.
- [29] D. Kendall, "Shape Manifolds, Procrustean Metrics and Complex Projective Spaces," *Bull. London Math. Soc.*, vol. 16, pp. 81-121, 1984.
- [30] J.J. Koenderink and A.J. van Doorn, "The Internal Representation of Solid Shape with Respect to Vision," *Biological Cybernetics*, vol. 32, pp. 211-216, 1979.
- [31] M. Lades, C. Vorbüggen, J. Buhmann, J. Lange, C. von der Malsburg, R. Wurtz, and W. Konen, "Distortion Invariant Object Recognition in the Dynamic Link Architecture," *IEEE Trans. Computers*, vol. 42, no. 3, pp. 300-311, Mar. 1993.
- [32] Y. Lamdan, J. Schwartz, and H. Wolfson, "Affine Invariant Model-Based Object Recognition," *IEEE Trans. Robotics and Automation*, vol. 6, pp. 578-589, 1990.
- [33] L.J. Latecki, R. Lakämper, and U. Eckhardt, "Shape Descriptors for Non-Rigid Shapes with a Single Closed Contour," *Proc. IEEE Conf. Computer Vision and Pattern Recognition*, pp. 424-429, 2000.
- [34] Y. LeCun, L. Bottou, Y. Bengio, and P. Haffner, "Gradient-Based Learning Applied to Document Recognition," *Proc. IEEE*, vol. 86, no. 11, pp. 2278-2324, Nov. 1998.
- [35] T.K. Leung, M.C. Burl, and P. Perona, "Finding Faces in Cluttered Scenes Using Random Labelled Graph Matching," *Proc. Fifth Int'l. Conf. Computer Vision*, pp. 637-644, 1995.
- [36] D.G. Lowe, "Object Recognition from Local Scale-Invariant Features," *Proc. Seventh Int'l. Conf. Computer Vision*, pp. 1150-1157, Sept. 1999.
- [37] J. Meinguet, "Multivariate Interpolation at Arbitrary Points Made Simple," *J. Applied Math. Physics (ZAMP)*, vol. 5, pp. 439-468, 1979.
- [38] B. Moghaddam, T. Jebara, and A. Pentland, "Bayesian Face Recognition," *Pattern Recognition*, vol. 33, no. 11, pp. 1771-1782, Nov. 2000.
- [39] F. Mokhtarian, S. Abbasi, and J. Kittler, "Efficient and Robust Retrieval by Shape Content Through Curvature Scale Space," *Image Databases and Multi-Media Search*, A.W.M. Smeulders and R. Jain, eds., pp. 51-58, World Scientific, 1997.
- [40] H. Murase and S. Nayar, "Visual Learning and Recognition of 3-D Objects from Appearance," *Int'l. J. Computer Vision*, vol. 14, no. 1, pp. 5-24, Jan. 1995.
- [41] M. Oren, C. Papageorgiou, P. Sinha, E. Osuna, and T. Poggio, "Pedestrian Detection Using Wavelet Templates," *Proc. IEEE Conf. Computer Vision and Pattern Recognition*, pp. 193-199, June 1997.
- [42] C. Papadimitriou and K. Stieglitz, *Combinatorial Optimization: Algorithms and Complexity*. Prentice Hall, 1982.
- [43] E. Persoon and K. Fu, "Shape Discrimination Using Fourier Descriptors," *IEEE Trans. Systems, Man and Cybernetics*, vol. 7, no. 3, pp. 170-179, Mar. 1977.
- [44] M.J.D. Powell, "A Thin Plate Spline Method for Mapping Curves into Curves in Two Dimensions," *Computational Techniques and Applications (CTAC '95)*, 1995.
- [45] B.D. Ripley, "Modelling Spatial Patterns," *J. Royal Statistical Society, Series B*, vol. 39, pp. 172-212, 1977.
- [46] B.D. Ripley, *Pattern Recognition and Neural Networks*. Cambridge Univ. Press, 1996.
- [47] E. Rosch, "Natural Categories," *Cognitive Psychology*, vol. 4, no. 3, pp. 328-350, 1973.
- [48] E. Rosch, C.B. Mervis, W.D. Gray, D.M. Johnson, and P. Boyes-Braem, "Basic Objects in Natural Categories," *Cognitive Psychology*, vol. 8, no. 3, pp. 382-439, 1976.
- [49] C. Schmid and R. Mohr, "Local Grayvalue Invariants for Image Retrieval," *IEEE Trans. Pattern Analysis and Machine Intelligence*, vol. 19, no. 5, pp. 530-535, May 1997.
- [50] S. Sclaroff and A. Pentland, "Modal Matching for Correspondence and Recognition," *IEEE Trans. Pattern Analysis and Machine Intelligence*, vol. 17, no. 6, pp. 545-561, June 1995.
- [51] G. Scott and H. Longuet-Higgins, "An Algorithm for Associating the Features of Two Images," *Proc. Royal Soc. London*, vol. 244, pp. 21-26, 1991.
- [52] L.S. Shapiro and J. M. Brady, "Feature-Based Correspondence: An Eigenvector Approach," *Image and Vision Computing*, vol. 10, no. 5, pp. 283-288, June 1992.
- [53] D. Sharvit, J. Chan, H. Tek, and B. Kimia, "Symmetry-Based Indexing of Image Databases," *J. Visual Comm. and Image Representation*, vol. 9, no. 4, pp. 366-380, Dec. 1998.
- [54] L. Sirovich and M. Kirby, "Low Dimensional Procedure for the Characterization of Human Faces," *J. Optical Soc. Am. A*, vol. 4, no. 3, pp. 519-524, 1987.
- [55] D.W. Thompson, *On Growth and Form*, Cambridge Univ. Press, 1917.
- [56] M. Turk and A. Pentland, "Eigenfaces for Recognition," *J. Cognitive Neuroscience*, vol. 3, no. 1, pp. 71-96, 1991.
- [57] S. Umeyama, "An Eigen Decomposition Approach to Weighted Graph Matching Problems," *IEEE Trans. Pattern Analysis and Machine Intelligence*, vol. 10, no. 5, pp. 695-703, Sept. 1988.
- [58] R.C. Veltkamp and M. Hagedoorn, "State of the Art in Shape Matching," Technical Report UU-CS-1999-27, Utrecht, 1999.
- [59] T. Vetter, M.J. Jones, and T. Poggio, "A Bootstrapping Algorithm for Learning Linear Models of Object Classes," *Proc. IEEE Conf. Computer Vision and Pattern Recognition*, pp. 40-46, 1997.
- [60] G. Wahba, *Spline Models for Observational Data*. Soc. Industrial and Applied Math., 1990.
- [61] A. Yuille, "Deformable Templates for Face Recognition," *J. Cognitive Neuroscience*, vol. 3, no. 1, pp. 59-71, 1991.
- [62] C. Zahn and R. Roskies, "Fourier Descriptors for Plane Closed Curves," *IEEE Trans. Computers*, vol. 21, no. 3, pp. 269-281, Mar. 1972.



**Serge Belongie** received the BS degree (with honor) in electrical engineering from the California Institute of Technology, Pasadena, California, in 1995, and the MS and PhD degrees in electrical engineering and computer sciences (EECS) at the University of California at Berkeley, in 1997 and 2000, respectively. While at Berkeley, his research was supported by a National Science Foundation Graduate Research Fellowship and the Chancellor's Opportunity Predoctoral Fellowship.

He is also a cofounder of Digital Persona, Inc., and the principal architect of the Digital Persona fingerprint recognition algorithm. He is currently an assistant professor in the Computer Science and Engineering Department at the University of California at San Diego. His research interests include computer vision, pattern recognition, and digital signal processing. He is a member of the IEEE.



**Jan Puzicha** received the Diploma degree in 1995 and the PhD degree in computer science in 1999, both from the University of Bonn, Bonn, Germany. He was with the Computer Vision and Pattern Recognition Group, University of Bonn, from 1995 to 1999. In September 1999, he joined the Computer Science Department, University of California, Berkeley, as an Emmy Noether Fellow of the German Science Foundation, where he is currently working on optimization methods for perceptual grouping and image segmentation. His research interests include computer vision, image processing, unsupervised learning, data analysis, and data mining.



**Jitendra Malik** received the BTech degree in electrical engineering from Indian Institute of Technology, Kanpur in 1980 and the PhD degree in computer science from Stanford University, Stanford, California, in 1986. In January 1986, he joined the faculty of the Computer Science Division, Department of EECS, University of California at Berkeley, where he is currently a professor. During 1995-1998, he also served as vice-chair for Graduate

Matters. He is a member of the Cognitive Science and Vision Science groups at UC Berkeley. His research interests are in computer vision and computational modeling of human vision. His work spans a range of topics in vision including image segmentation and grouping, texture, stereopsis, object recognition, image-based modeling and rendering, content-based image querying, and intelligent vehicle highway systems. He has authored or coauthored more than 100 research papers on these topics. He received the gold medal for the best graduating student in electrical engineering from IIT Kanpur in 1980, a Presidential Young Investigator Award in 1989, and the Rosenbaum fellowship for the Computer Vision Programme at the Newton Institute of Mathematical Sciences, University of Cambridge in 1993. He received the Diane S. McEntyre Award for Excellence in Teaching from the Computer Science Division, University of California at Berkeley, in 2000. He is an Editor-in-Chief of the *International Journal of Computer Vision*. He is a member of the IEEE.

► **For more information on this or any other computing topic, please visit our Digital Library at <http://computer.org/publications/dlib>.**